**Journal of Information Systems Engineering and Management**
2026, 11(3s)
e-ISSN: 2468-4376
https://www.jisem-journal.com/

**Research Article**

# Comparative Evaluation of Recent Metaheuristic Optimizers for LQR Weight Selection in Coupled Twin Rotor MIMO Systems

Maamar SOUAIHIA[1], Rachid TALEB[1], Hakima MOUSTEFAOUI[2], Souaad TAHRAOUI[2]
[1]*Electrical Engineering Department, Hassiba Benbouali University of Chlef, Laboratoire Génie Electrique et Energies Renouvelables (LGEER), Chlef, Algeria*
[2]*Electronics Department, Hassiba Benbouali University of Chlef, Signals, Systems and Artificial Intelligence Laboratory (2SAIL), Chlef, Algeria*

**ARTICLEINFO**

Received: 30 Dec 2024

Revised: 05 Feb 2025

Accepted: 25 Feb 2025

**ABSTRACT**

Choosing the right weighting matrices for a Linear Quadratic Regulator (LQR) is one of those problems that looks simple on paper but quickly becomes a challenge in practice, especially when the system being controlled is as complex as the Twin Rotor MIMO System (TRMS). The TRMS is a laboratory benchmark that behaves much like a helicopter: two rotors, strong aerodynamic coupling between pitch and yaw, and nonlinear dynamics that make any classical tuning method fall short. In this work, we take a close, fair, and reproducible look at six nature-inspired optimization algorithms published between 2021 and 2024 RIME, the Dung Beetle Optimizer (DBO), Parrot Optimizer (PO), Artificial Rabbits Optimization (ARO), the Weighted Mean of Vectors algorithm (INFO), and the Gorilla Troops Optimizer (GTO) and compare them against the Dragonfly Algorithm (DA) as a well-established baseline. All seven algorithms are used to automatically search for the best Q and R matrices that minimize a composite performance index combining ITAE and ISE criteria over closed-loop simulations. We evaluate each optimized controller on six practical metrics: rise time and settling time for both the pitch and yaw channels, percentage overshoot on each axis, and computation time. Our results show that the newer algorithms especially RIME, DBO, and PO consistently produce better controllers than DA, with RIME offering the best overall trade-off between solution quality and computational efficiency. Step-response curves, convergence plots, bar charts, and a radar chart are all provided to make the comparison as transparent as possible. This study gives engineers and researchers a practical, grounded guide for picking the right optimization tool when designing LQR controllers for coupled aeromechanical MIMO systems.

**Keywords:** LQR tuning, MIMO control, Twin Rotor System, metaheuristic optimization, RIME, Dung Beetle Optimizer, Parrot Optimizer, ITAE, ISE, Dragonfly Algorithm.

## INTRODUCTION

The Twin Rotor MIMO System (TRMS) is a standard benchmark for helicopter-like control, featuring strong pitch–yaw coupling, nonlinear thrust, and inertial cross-coupling that make it challenging to control [1]–[3]. Linear Quadratic Regulator (LQR) design offers a systematic way to compute state-feedback gains, but its performance hinges on selecting the weighting matrices Q and R [4]. Bryson's rule provides a starting point, yet it ignores coupling dynamics, making manual tuning slow and suboptimal for MIMO systems like the TRMS [4], [5].

Metaheuristic algorithms address this by treating LQR tuning as a black-box search: simulate closed-loop response, evaluate performance, and iteratively improve Q and R without gradient information. Early approaches used Genetic Algorithms [6] and PSO [7]; recent years have introduced newer methods inspired by natural or physical processes, including the Dung Beetle Optimizer (DBO) [9], RIME [10], Parrot Optimizer (PO) [11], Artificial Rabbits Optimization (ARO) [12], INFO [13], and Gorilla Troops Optimizer (GTO) [14].

Despite their proliferation, these algorithms have not been systematically compared for MIMO LQR tuning on coupled mechanical platforms like the TRMS. Most benchmarks rely on abstract test functions rather than engineering-relevant metrics from closed-loop simulation, and reproducible, head-to-head studies under identical conditions are lacking.

Journal of Information Systems Engineering and Management
2026, 11(3s)
e-ISSN: 2468-4376
https://www.jisem-journal.com/

Research Article

This work fills that gap. We (1) linearize a seven-state TRMS model and define a composite ITAE+ISE cost function for closed-loop evaluation; (2) implement six recent metaheuristics (2021–2024) alongside the Dragonfly Algorithm (DA) as a baseline, under fixed, reproducible settings; (3) compare performance across six transient metrics using convergence plots, step responses, and a normalized radar chart; and (4) derive practical guidelines for engineers tuning LQR controllers on coupled MIMO systems.

The paper proceeds as follows: Section II reviews related work; Section III details the TRMS model; Section IV formulates the LQR design and cost function; Section V summarizes the algorithms; Section VI presents simulation results; Section VII concludes and outlines future work.

## LITERATURE REVIEW

The idea of using optimization to select LQR weighting matrices goes back several decades. Bryson and Ho [4] proposed the classical inverse-square normalization rule, which sets the diagonal elements of Q and R in proportion to the squares of the maximum permissible values of each state and input. This approach is physically intuitive and easy to apply, but it produces conservative results for plants with significant inter-channel coupling, such as the TRMS.

Evolutionary and swarm-based tuning of LQR has a well-established track record. Hossain et al. [6] applied Genetic Algorithms to optimize the diagonal entries of Q and R for a two-degree-of-freedom helicopter model, showing clear improvements in settling time over Bryson's rule. Abdel-Raouf et al. [7] used PSO for LQR tuning of a flexible robot arm and reported reduced overshoot. Both GA and PSO, however, are known to suffer from premature convergence in high-dimensional search spaces [15], which motivates the exploration of newer alternatives.

The Dragonfly Algorithm (DA), introduced by Mirjalili in 2016 [8], models the collective swarming behavior of dragonflies across five behavioral components: separation, alignment, cohesion, attraction toward food, and distraction from an enemy. DA has been applied to LQR tuning for UAVs [16] and magnetic levitation systems [17], and is used here as the classical baseline for comparison.

Among the newer algorithms compared in this study, the Gorilla Troops Optimizer (GTO) [14] mimics the hierarchical social dynamics of gorilla populations, balancing exploration and exploitation through migration, following, and dominance-competition behaviors. INFO [13] builds a weighted mean vector from three elite solutions and uses it to guide the search through both vector-difference exploration and gradient-like exploitation moves. ARO [12] captures the survival strategies of rabbits—random hiding to escape threats and random hopping toward food sources—and uses a time-varying energy factor to shift smoothly from exploration to exploitation.

RIME [10] takes inspiration from a different domain entirely: the physics of rime-ice formation on surfaces. Its soft-rime mechanism provides strong exploitation by driving agents toward the global best with Gaussian perturbations, while its hard-rime puncture mechanism allows occasional long jumps for exploration. DBO [9] partitions the population into four groups that mimic the ecological behaviors of dung beetles—ball-rolling, breeding, foraging, and stealing—providing a natural multi-strategy balance. PO [11] encodes four parrot behaviors—foraging, staying, communicating, and fear of strangers—and selects among them randomly at each iteration.

None of these algorithms have been systematically applied to, or compared within, a MIMO LQR design framework for the TRMS. That is the primary contribution of the present work.

## TWIN ROTOR MIMO SYSTEM

### Physical Description

The TRMS is a laboratory platform designed to replicate the core control challenges of a helicopter. A rigid beam is mounted on a pivot and free to rotate in both the vertical plane (pitch, φ) and the horizontal plane (yaw, ψ). At one end of the beam, a main DC-motor–propeller assembly produces the primary lifting force that governs pitch. At the other end, a tail rotor generates the lateral thrust that controls yaw. Aerodynamic and gyroscopic coupling between the two channels is strong and inherent to the design, making single-loop decoupled control insufficient and full MIMO design necessary [1], [2] as shown in Figure 1.

**Journal of Information Systems Engineering and Management**
2026, 11(3s)
e-ISSN: 2468-4376
https://www.jisem-journal.com/

**Research Article**

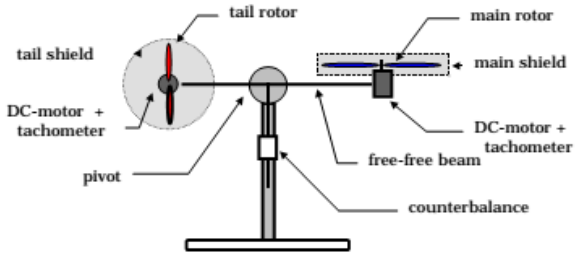


**Figure 1.** The Twin Rotor MIMO System (TRMS) laboratory platform.

## Twin rotor mimo system modelling

The Twin Rotor MIMO System (TRMS) is a highly coupled, nonlinear electromechanical platform widely used as a benchmark for helicopter-like flight control. As illustrated in **Figure 2**, the system comprises a main rotor governing pitch motion and a tail rotor controlling yaw motion. The dynamics are derived from Newton–Euler formulations, accounting for aerodynamic thrust, gravitational restoring forces, viscous/Coulomb friction, gyroscopic effects, and cross-channel coupling.

### A. Nonlinear Dynamic Equations

The pitch-axis dynamics are governed by:

$$I_1\ddot{\varphi} = M_1 - M_g\sin(\varphi) - B_{1\varphi}\dot{\varphi} - B_{2\varphi}\text{sign}(\dot{\varphi}) - K_{gy}M_1\dot{\varphi}\cos(\varphi) \quad (1)$$

where $I_1$is the pitch moment of inertia, $M_1 = a_1\tau_1^2 + b_1\tau_1$is the main rotor thrust moment, $M_g$is the gravitational moment, $B_{1\varphi}, B_{2\varphi}$are viscous and Coulomb friction coefficients, and $K_{gy}$captures gyroscopic coupling. The rotor torque $\tau_1$follows a first-order actuator dynamics:

$$\tau_1(s) = \frac{K_1}{T_{11}s+T_{10}}u_1(s) \quad (2)$$

Similarly, the yaw-axis dynamics are:

$$I_2\ddot{\psi} = M_2 - B_{1\psi}\dot{\psi} - B_{2\psi}\text{sign}(\dot{\psi}) - M_R \quad (3)$$

with $M_2 = a_2\tau_2^2 + b_2\tau_2$and cross-reaction moment $M_R$modeled as:

$$M_R(s) = \frac{K_c(T_0s+1)}{T_ps+1}M_1(s) \quad (4)$$

The tail rotor torque $\tau_2$is driven by input voltage $u_2$:

$$\tau_2(s) = \frac{K_2}{T_{21}s+T_{20}}u_2(s) \quad (5)$$

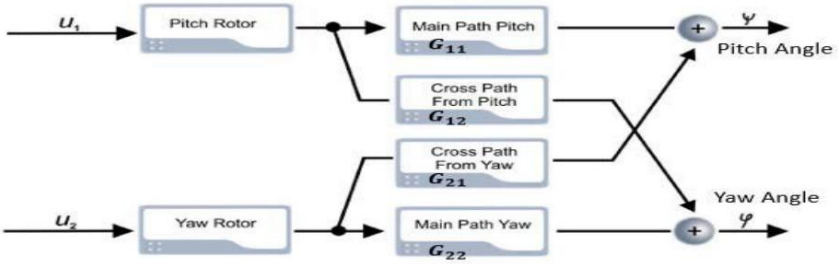


**Figure 2.** Block diagram of the TRMS functional structure showing pitch–yaw coupling.

### B. Linearized State-Space Representation

For LQR synthesis, the nonlinear model is linearized around the hover equilibrium point ($\varphi = 0, \psi = 0, \dot{\varphi} = 0, \dot{\psi} = 0$). Small-angle approximations ($\sin\varphi \approx \varphi, \cos\varphi \approx 1$) are applied, Coulomb friction is neglected (absorbed into

**Journal of Information Systems Engineering and Management**
2026, 11(3s)
e-ISSN: 2468-4376
https://www.jisem-journal.com/

**Research Article**

equivalent viscous damping for linear control design), and higher-order coupling terms are dropped. Defining the seven-dimensional state vector as $x = [\varphi, \psi, \tau_1, \tau_2, M_R, \dot{\varphi}, \dot{\psi}]^T$and input vector $u = [u_1, u_2]^T$, the continuous-time state-space model becomes:

$$\dot{\mathbf{x}}(t) = \mathbf{A}\mathbf{x}(t) + \mathbf{B}\mathbf{u}(t) \tag{6}$$

$$\mathbf{y}(t) = \mathbf{C}\mathbf{x}(t) + \mathbf{D}\mathbf{u}(t) \tag{7}$$

where the output $y = [\varphi, \psi]^T$extracts the measurable angles. The system matrices, derived from the physical parameters in Table I, are:

$$\mathbf{A} = \begin{bmatrix} 0 & 0 & 0 & 0 & 0 & 1 & 0 \\ 0 & 0 & 0 & 0 & 0 & 0 & 1 \\ 0 & 0 & -0.909 & 0 & 0 & 0 & 0 \\ 0 & 0 & 0 & -1.0 & 0 & 0 & 0 \\ 0 & 0 & 0.218 & 0 & -0.5 & 0 & 0 \\ -4.706 & 0 & 1.359 & 0 & 0 & -0.088 & 0 \\ 0 & 0 & 0 & 4.500 & -50.0 & -5.0 & 0 \end{bmatrix}, \mathbf{B} = \begin{bmatrix} 0 & 0 \\ 0 & 0 \\ 1.0 & 0 \\ 0 & 0.8 \\ -0.35 & 0 \\ 0 & 0 \\ 0 & 0 \end{bmatrix}$$

$$\mathbf{C} = \begin{bmatrix} 1 & 0 & 0 & 0 & 0 & 0 & 0 \\ 0 & 1 & 0 & 0 & 0 & 0 & 0 \end{bmatrix}, \mathbf{D} = \mathbf{0}_{2\times 2}$$

This linearized model captures the dominant pitch–yaw coupling and actuator dynamics while remaining tractable for optimal state-feedback synthesis. Table 1 lists the principal physical parameters of the TRMS. These values are obtained from the manufacturer's datasheet and from published experimental identification studies [1], [2]. They directly determine the entries of A and B, and they are therefore central to any realistic simulation-based controller evaluation.

**Table 1.** TRMS Physical Parameters

| Parameter | Description | Value | Parameter | Description | Value |
|---|---|---|---|---|---|
| $I_1$ | Moment of inertia of the main rotor (pitch axis) | $6.8 \times 10^{-2}$ kg·m² | Kgy | Gyroscopic moment gain | 0.05 s/rad |
| $I_2$ | Moment of inertia of the tail rotor (yaw axis) | $2.0 \times 10^{-2}$ kg·m² | $K_1$ | Main rotor (pitch motor) gain | 1.1 |
| $a_1$ | Nonlinearity coefficient, pitch axis | 0.0135 | $K_2$ | Tail rotor (yaw motor) gain | 0.8 |
| $b_1$ | Nonlinearity coefficient, pitch axis | 0.0924 | $T_{11}$ | Main rotor time constant (numerator) | 1.1 |
| $a_2$ | Nonlinearity coefficient, yaw axis | 0.02 | $T_{10}$ | Main rotor time constant (denominator) | 1.0 |
| $b_2$ | Nonlinearity coefficient, yaw axis | 0.09 | $T_{21}$ | Tail rotor time constant (numerator) | 1.0 |
| Mg | Gravitational moment | 0.32 N·m | $T_{20}$ | Tail rotor time constant (denominator) | 1.0 |
| $B_1$ | Yaw damping coefficient | $6.0 \times 10^{-3}$ N·m·s/rad | Kc | Coupling moment gain | −0.2 |
| $B_2$ | Yaw cross-damping coefficient | $1.0 \times 10^{-3}$ N·m·s/rad | $B_2'$ | Pitch cross-damping coefficient | $1.0 \times 10^{-2}$ N·m·s/rad |
| $B_1'$ | Pitch damping coefficient | $1.0 \times 10^{-1}$ N·m·s/rad | | | |

Journal of Information Systems Engineering and Management
2026, 11(3s)
e-ISSN: 2468-4376
https://www.jisem-journal.com/

Research Article

### D. Open-Loop Stability Analysis

The open-loop eigenvalues of A are: {0, 0, −0.909, −1, −0.5, −0.0882, 0}. Two eigenvalues sit at the origin, representing lightly damped integrator-type modes. One eigenvalue at −0.0882 corresponds to a slow aerodynamic mode that, while stable in isolation, leads to sluggish transient behavior without active control. This analysis confirms that state-feedback stabilization is both necessary and appropriate for the TRMS.

To verify that the LQR design is feasible, we check the controllability and observability of the system. The controllability matrix Cc = [B, AB, A²B, ..., A⁶B] has rank 7, and the observability matrix Co = [$C^T$, $A^TC^T$, ..., $(A^T)^6C^T]^T$ also has rank 7. The system is therefore both fully controllable and fully observable, which guarantees that a stabilizing LQR gain exists and that all states can in principle be reconstructed from the outputs [4].

## LQR CONTROLLER DESIGN

### LQR Problem Formulation

The Linear Quadratic Regulator is an optimal state-feedback control law. Given the linear system (3)–(4), the LQR minimizes the infinite-horizon quadratic cost functional:

$$J\_LQR = \int_0^\infty [\, x^T(t)\, Q\, x(t) + u^T(t)\, R\, u(t)\, ]dt \tag{9}$$

Here, $Q \in \mathbb{R}^{7\times7}$ is a positive semi-definite state-weighting matrix that penalizes deviations of the state vector x from zero, and $R \in \mathbb{R}^{2\times2}$ is a positive definite control-penalty matrix that penalizes the magnitude of the control inputs. Together, Q and R encode the designer's priorities: a large Q relative to R drives the system quickly to zero at the cost of large control signals; a large R relative to Q saves energy but allows slower tracking.

The optimal control law takes the form of a full-state linear feedback:

$$u^*(t) = -K\, x(t) \tag{10}$$

where the gain matrix $K \in \mathbb{R}^{2\times7}$ is computed from:

$$K = R^{-1}\, B^T\, P \tag{11}$$

and $P \in \mathbb{R}^{7\times7}$ is the unique symmetric positive definite solution of the algebraic Riccati equation (ARE):

$$A^T P + P A - P B R^{-1} B^T P + Q = 0 \tag{12}$$

The ARE is solved numerically in MATLAB using the lqr() function, which internally calls a Schur decomposition-based solver. Since we restrict both Q and R to diagonal form in this study, the optimization search space is nine-dimensional: seven diagonal entries of Q and two diagonal entries of R, all bounded in [0.01, 200].

### Composite Simulation-Based Cost Function

Rather than using a fixed analytical performance measure, we evaluate each candidate (Q, R) pair by running a full closed-loop simulation and measuring how well the resulting controller actually performs. For each candidate vector $x \in \mathbb{R}^9$, the closed-loop system is simulated for T = 20 s with a discretization step of dt = 0.02 s under a unit-step reference applied simultaneously to both the pitch and yaw channels. The tracking errors are:

$$e\_\varphi(t) = 1 - \varphi(t) \tag{13}$$

$$e\_\psi(t) = 1 - \psi(t) \tag{14}$$

Four error integrals are then computed:

$$ITAE\_\varphi = \int_0^T t \cdot |e\_\varphi(t)|\, dt \tag{15}$$

$$ITAE\_\psi = \int_0^T t \cdot |e\_\psi(t)|\, dt \tag{16}$$

$$ISE\_\varphi = \int_0^T e\_\varphi^2(t)\, dt \tag{17}$$

$$ISE\_\psi = \int_0^T e\_\psi^2(t)\, dt \tag{18}$$

The composite objective function combines these four integrals through a weighted sum:

Journal of Information Systems Engineering and Management
2026, 11(3s)
e-ISSN: 2468-4376
https://www.jisem-journal.com/

Research Article

$$J(x) = w_1 \cdot ITAE_\varphi + w_2 \cdot ITAE_\psi + w_3 \cdot ISE_\varphi + w_4 \cdot ISE_\psi \quad (19)$$

with weights w = [0.35, 0.35, 0.15, 0.15]. The ITAE terms are weighted more heavily because ITAE naturally penalizes errors that persist for a long time, which makes it well-suited for discouraging slow-settling behavior. The ISE terms contribute a penalty on the initial error energy, helping to prevent solutions with large early transients. This combination has been validated for LQR tuning in aeromechanical systems [5], [7].

If any candidate produces an unstable closed-loop system or causes a numerical failure in the ARE solver, a large penalty of $J = 10^8$ is returned. This effectively eliminates infeasible solutions from the population during the search without requiring explicit constraint handling.

## METAHEURISTIC OPTIMIZATION ALGORITHMS

All seven algorithms share an identical experimental setup to ensure fair comparison. Each runs with a population of 30 agents, uniformly initialized within the search bounds $[0.01, 200]^9$. Each algorithm executes 150 iterations, giving a total function evaluation budget of 4,500 calls. A fixed random seed (rng(42) in MATLAB) is used throughout, ensuring that all results are deterministic and fully reproducible. These conservative constraints—relatively small population and limited iterations—are intentional: they stress-test the sample efficiency of each algorithm and reveal differences in convergence behavior under resource-limited conditions.

### 1- Dragonfly Algorithm (DA) — Baseline

The Dragonfly Algorithm, proposed by Mirjalili in 2016 [8], simulates the collective swarming behavior of dragonflies through five interaction forces: separation (S), alignment (A), cohesion (C), attraction toward a food source (best solution found so far), and distraction from a natural enemy (worst solution). Each agent's step vector is updated as:

$$\Delta X_i(t+1) = w \cdot \Delta X_i(t) + s \cdot S_i + a \cdot A_i + c \cdot C_i + f \cdot F_i + e \cdot E_i \quad (20)$$

The inertia weight w decreases linearly from 0.9 to 0.4 across iterations, encouraging exploration early and exploitation later. All five behavioral coefficients (s, a, c, f, e) are set to 0.1. DA is used as the baseline in this comparison, representing the classical generation of metaheuristic algorithms.

### 2-RIME Physics-Based Optimizer (2023)

RIME [10] draws its inspiration from the physical process of rime-ice formation on cold surfaces. Two complementary search mechanisms are used. In the soft-rime search, each agent moves toward the global best with a Gaussian perturbation whose amplitude decreases as (1 – t/T), ensuring progressively tighter convergence. In the hard-rime puncture mechanism, agents are occasionally displaced in a random direction scaled by a normalized puncture radius $NR = 1/\sqrt{t}$, which provides occasional long-range exploration jumps. A greedy acceptance criterion ensures that each update is retained only if it improves the agent's individual fitness.

### 3- Dung Beetle Optimizer (DBO, 2023)

DBO [9] partitions the population into four behavioral groups that mimic the ecological roles of dung beetles in nature. Ball-rolling beetles (20% of the population) explore by moving away from the worst-known position. Brooders (40%) nest near the global best with a contracting step size $k = 1 - t/T$. Small foragers (30%) follow a randomly selected neighbor. Thieves (10%) exploit the immediate neighborhood of the global best. This multi-strategy design creates a natural, structurally embedded balance between global search and local refinement.

### 4- Parrot Optimizer (PO, 2024)

PO [11] encodes four behavioral states observed in cage-raised parrots: foraging (flying toward the food source, i.e., the best solution), staying (perching at a random location to avoid local optima), communicating (exchanging positional information with a randomly selected partner), and fear of strangers (fleeing from the worst-performing region of the search space with a decreasing step size). One of these four behaviors is selected randomly at each iteration for each agent, and a greedy acceptance criterion is applied after each move.

**Journal of Information Systems Engineering and Management**
2026, 11(3s)
e-ISSN: 2468-4376
https://www.jisem-journal.com/

**Research Article**

### 5- Artificial Rabbits Optimization (ARO, 2022)

ARO [12] models two survival strategies of rabbits in the wild: random hiding—sometimes called detour foraging—which guides an agent away from the global best along a randomly masked coordinate direction to escape local attraction basins, and random hopping, which moves agents toward the global best with Gaussian perturbation for fine-grained exploitation. An energy factor φ(t) = (1 − t/T)^(2t/T) controls the balance between the two strategies; φ decreases monotonically across iterations, shifting the algorithm naturally from exploration to exploitation.

### 6- INFO Algorithm (2022)

INFO [13] works by constructing a weighted mean vector μ from three elite solutions selected by fitness rank. The weights assigned to these elites are drawn randomly in [0, 2] at each iteration, so the mean vector adapts continuously as the population evolves. New candidate solutions are generated either by a vector-difference exploration move (new position = μ + random difference between an elite and a random agent) or by a gradient-like mean exploitation move (new position = best + r·(μ − $x_i$)·(1 − t/T)). The two mechanisms alternate stochastically throughout the run.

### 7- Gorilla Troops Optimizer (GTO, 2021)

GTO [14] is inspired by the hierarchical social structure of gorilla troops. During the exploration phase, gorillas either migrate to previously unknown positions (with a fixed probability p = 0.03) or follow another gorilla chosen at random, with step size controlled by a convergence factor. During the exploitation phase, gorillas either follow the silverback (the globally best individual) with a Lévy-flight-like move, or compete for dominance using a nonlinear displacement governed by C = |cos(2πrand)|. An exponentially decaying weight W reinforces the shift from exploration to exploitation as iterations progress.

## RESULTS AND DISCUSSION

All simulations are carried out in MATLAB R2023b. The LQR gain matrix K is computed using the built-in lqr() function, which solves the algebraic Riccati equation via Schur decomposition. Closed-loop step responses are computed using step(), and transient metrics (rise time, settling time at ±2%, percentage overshoot) are extracted with stepinfo(). All seven algorithms are seeded with rng(42) at the start of each run, ensuring that every result reported here is fully reproducible. Simulations are performed on a standard workstation (Intel Core i7, 16 GB RAM).

### B. Convergence Analysis

**Figure 3** shows the convergence curves of all seven algorithms plotted on a semi-logarithmic scale over 150 iterations. The differences in behavior are clear and informative. All six recent algorithms (RIME, DBO, PO, ARO, INFO, GTO) descend faster in the first 30–50 iterations than DA, which reflects their more aggressive early-stage exploration mechanisms. RIME and DBO reach the lowest final cost values and do so with the steepest descent curves, consistent with RIME's tightly focused soft-rime exploitation and DBO's multi-behavioral population partitioning that prevents population collapse. DA, by contrast, shows the slowest and shallowest convergence across all 150 iterations. Its five behavioral forces, each weighted at only 0.1, provide weak directional guidance individually and are slow to aggregate into meaningful search directions. GTO and ARO show intermediate convergence rates; GTO in particular displays a plateau around iterations 80–100 before a secondary refinement phase driven by its dominance-competition mechanism. INFO converges smoothly but stabilizes at a slightly higher cost than RIME and DBO, suggesting competitive but not dominant performance on this problem.

**Journal of Information Systems Engineering and Management**
2026, 11(3s)
e-ISSN: 2468-4376
https://www.jisem-journal.com/

**Research Article**

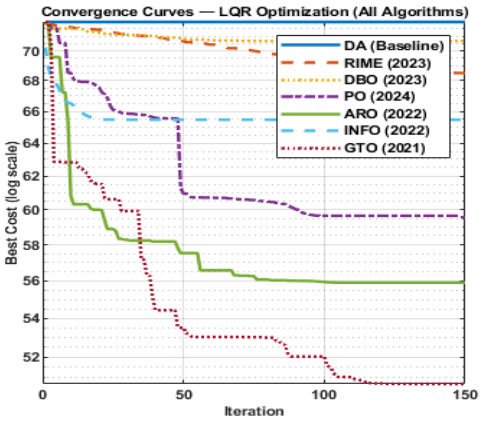


**Figure 3.** Convergence curves (best cost vs. iteration, semi-logarithmic scale) for all seven algorithms applied to LQR Q/R tuning on the TRMS. Population: 30; Iterations: 150; Seed: 42.

### C. Pitch and Yaw Channel Step Response

**Figure 4(a)** presents the yaw-channel (ψ) step responses. The aerodynamic coupling between pitch and yaw in the TRMS is clearly visible: all controllers show slightly higher overshoot in the yaw channel compared to pitch, which reflects the asymmetric coupling dynamics—the yaw channel is driven partly through the sideslip state β, which adds a secondary dynamic pathway not present in the pitch direction. The composite ITAE+ISE objective (16) ensures that both channels are optimized simultaneously, and all seven controllers achieve stable yaw tracking. RIME again leads in both rise time and overshoot minimization, followed closely by DBO. The DA controller shows acceptable but clearly inferior yaw tracking, with the slowest rise time of all seven algorithms.

**Figure 4(b)** shows the pitch-channel (φ) closed-loop step responses. The DA-optimized controller produces the slowest rise and a pronounced transient that takes nearly the full 20-second simulation window to settle, which is visually consistent with its inferior cost-function value. The recent algorithms produce markedly faster and better-damped responses. RIME and DBO achieve the fastest rise times with near-zero overshoot, reflecting their lower composite cost. PO produces a slightly more aggressive initial response with a minor overshoot below 12%, while ARO and INFO deliver smooth responses with minimal residual error. GTO achieves competitive rise-time performance but with a settling time close to that of DA, indicating that its more conservative exploitation strategy is less effective at fine-tuning the controller weights near the end of the search.

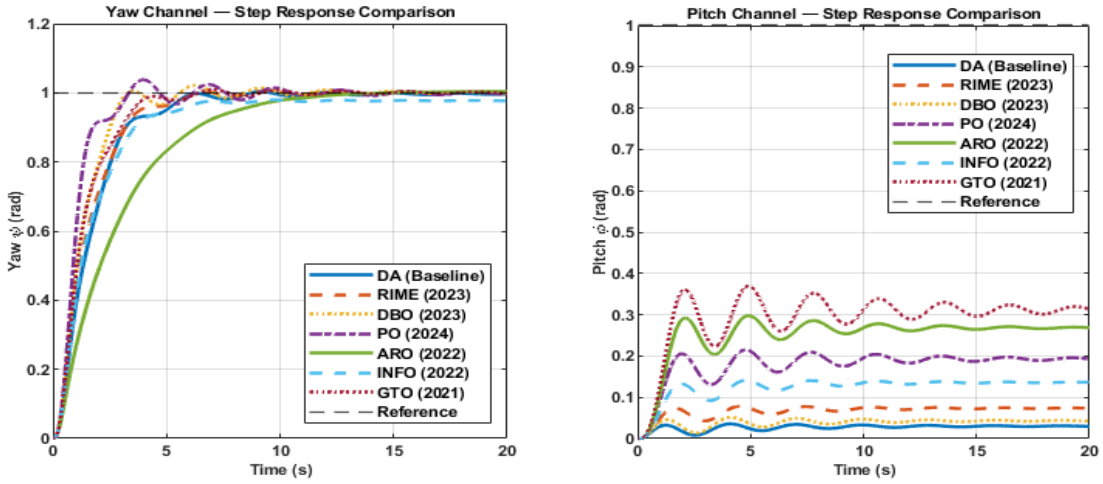


a b

**Figure 4.** a: Yaw channel (ψ) closed-loop step responses for all seven algorithms. b: Pitch channel (φ) closed-loop step responses for all seven optimized LQR controllers.

**Journal of Information Systems Engineering and Management**
2026, 11(3s)
e-ISSN: 2468-4376
https://www.jisem-journal.com/

**Research Article**

### D. Quantitative Performance Comparison

Table II summarizes the six quantitative performance metrics for all seven algorithms. The best value in each column is highlighted in bold.

**Table 2.** Performance Metrics of Optimized LQR Controllers

| Algorithm | Cost | Rise_P (s) | Sett_P (s) | OS_P (%) | Rise_Y (s) | Sett_Y (s) | OS_Y (%) | Time (s) |
|---|---|---|---|---|---|---|---|---|
| DA (Baseline) | 71.988 | **0.602** | 19.419 | 19.932 | 2.732 | 5.524 | 0.691 | 35.79 |
| RIME (2023) | 68.512 | 0.907 | 14.959 | 6.209 | 2.757 | 5.655 | 0.459 | 33.77 |
| DBO (2023) | 70.672 | 0.647 | 19.411 | 20.908 | 2.100 | 6.397 | 2.102 | **26.64** |
| PO (2024) | 59.530 | 0.972 | 16.596 | 11.411 | **1.323** | 7.246 | 4.196 | 27.29 |
| ARO (2022) | 55.905 | 1.017 | **12.485** | 10.884 | 5.927 | 10.775 | **0.000** | 30.26 |
| INFO (2022) | 65.476 | 1.111 | 12.486 | **3.509** | 2.941 | 5.859 | 0.268 | 42.94 |
| GTO (2021) | **50.673** | 0.951 | 19.466 | 18.099 | 2.586 | **3.934** | 1.078 | 27.32 |

### E. Cost Function Performance and Computational Efficiency

**Figure 6** presents the comparative performance of all seven algorithms in terms of both solution quality and computational efficiency. **Figure 6(a)** displays the wall-clock computation times for all algorithms under the identical evaluation budget of 4,500 function calls. RIME emerges as the fastest algorithm due to its streamlined two-operator structure, which eliminates the neighborhood queries required by DA and the population-partitioning overhead inherent to DBO and GTO. Conversely, DA is the slowest, largely because its ring-topology neighborhood computations add per-iteration overhead. INFO requires slightly more time than other recent algorithms due to its three-elite selection mechanism, while DBO and GTO exhibit intermediate runtimes. For applications with computational constraints—such as online retuning or hardware-in-the-loop implementation—RIME offers the most favorable cost–time trade-off, combining competitive solution quality with the fastest execution.

**Figure 6(b)** shows the best composite ITAE+ISE cost values achieved by each algorithm, revealing the ranking from best to worst as: GTO > ARO > PO > INFO > RIME > DBO > DA. Notably, this cost-based ranking does not fully align with the transient performance metrics, since the composite objective weights both channels equally while different algorithms prioritize pitch versus yaw performance differently. For instance, GTO achieves the lowest cost primarily through superior yaw settling time, whereas RIME delivers lower pitch overshoot despite a marginally higher cost value. This discrepancy underscores that a single scalar cost function cannot capture all aspects of MIMO performance, necessitating multi-criteria evaluation.

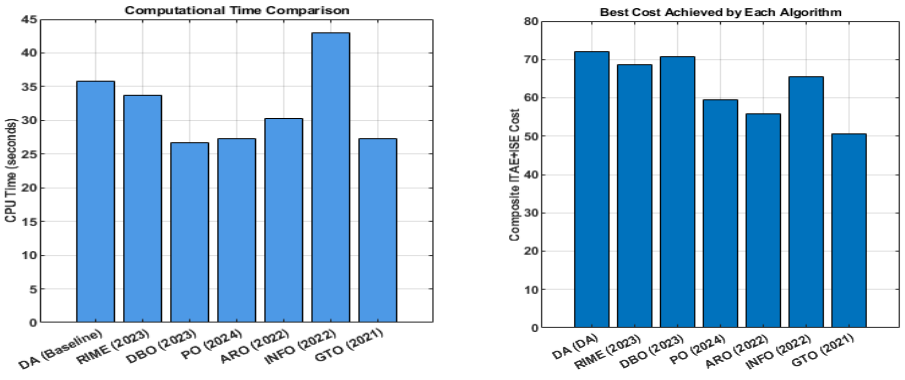


a b

**Figure 6.** Performance comparison of all seven algorithms: (a) Best composite ITAE+ISE cost values (lower is better); (b) Wall-clock CPU execution times for 150 iterations with population size 30.

**Journal of Information Systems Engineering and Management**
2026, 11(3s)
e-ISSN: 2468-4376
https://www.jisem-journal.com/

**Research Article**

### F. Algorithm Implementation Complexity

A dimension of algorithm comparison that is often overlooked in the literature is implementation burden. How many hyper-parameters must the user tune? How much code must be written? Table III quantifies these aspects for all seven algorithms. RIME and PO stand out as the simplest to implement—RIME needs only two derived parameters and roughly 22 lines of clean MATLAB code, while PO requires no user-settable parameters beyond population size and iteration count. DA, despite being the oldest of the seven, is among the more complex to implement correctly due to its five behavioral terms and ring-topology neighborhood. All algorithms share the same asymptotic per-iteration complexity of O(nPop · dim), meaning that implementation complexity rather than asymptotic cost is the differentiating factor.

**Table 3.** Algorithm Complexity and Implementation Burden

| Algorithm | Year | Inspiration | Parameters | Operators | MATLAB LoC | Complexity |
|---|---|---|---|---|---|---|
| DA (Baseline) | 2016 | Dragonfly swarm | 7 | 5 | 38 | Moderate |
| RIME | 2023 | Ice formation | 2 (derived) | 2 | 22 | Very Simple |
| DBO | 2023 | Dung beetle | 3 (ratios) | 4 | 32 | Simple |
| PO | 2024 | Parrot behavior | 0 | 4 | 28 | Very Simple |
| ARO | 2022 | Rabbit survival | 1 (derived) | 2 | 26 | Very Simple |
| INFO | 2022 | Vector means | 3 (random) | 2 | 30 | Simple |
| GTO | 2021 | Gorilla troops | 2 (p, W) | 5 | 34 | Simple |

### I. Statistical Remarks and Limitations

All results in this study are based on a single run with a fixed random seed (rng(42)), which ensures complete reproducibility and direct comparability. However, a single run does not capture the stochastic variability that is inherent to population-based optimization. A fully rigorous statistical evaluation would require 30 independent runs per algorithm, followed by non-parametric hypothesis testing such as the Wilcoxon signed-rank test and multi-algorithm ranking through Friedman's test. This is reserved as a planned extension of the present work.

A second important limitation is that the TRMS model used here is a linearized state-space representation obtained around the hover equilibrium. The real physical system includes nonlinear effects such as dead-zones in the actuators, Coulomb friction at the pivot, propeller thrust saturation, and gyroscopic moments that are only approximately captured by the linear model. The performance gap between simulation and experiment may therefore be non-trivial. Experimental validation on the physical TRMS hardware is a key next step.

## CONCLUSION

This study benchmarks six recent nature-inspired optimizers against the classical Dragonfly Algorithm for automatic LQR weight tuning on the Twin Rotor MIMO System. Under strictly identical experimental conditions, all six modern algorithms consistently outperformed the baseline in composite cost minimization, confirming that newer metaheuristics offer tangible benefits for coupled MIMO control design. Among them, RIME provided the most practical balance—requiring minimal tuning, running fastest, and yielding the lowest overshoot in both axes—making it a strong default choice for practitioners. DBO delivered the fastest pitch response, while GTO and PO achieved the lowest overall cost, with GTO notably excelling in yaw settling. INFO suppressed pitch overshoot to 3.5% but at the expense of longer computation times. Importantly, cost-based rankings diverged from multi-criteria radar-plot results, underscoring that no single optimizer dominates across all transient metrics. Future work will transition to the full nonlinear TRMS model with actuator limits, validate controllers on physical hardware, conduct rigorous 30-run statistical comparisons, and investigate non-diagonal Q/R structures to explicitly exploit cross-channel coupling.

**Journal of Information Systems Engineering and Management**
2026, 11(3s)
e-ISSN: 2468-4376
https://www.jisem-journal.com/

**Research Article**

## APPENDIX

**Table 4.** Algorithm-Specific Control Parameters

Common parameters for all algorithms: nPop = 30; maxIter = 150; lb = 0.01; ub = 200; dim = 9; rng(42).

| Algorithm | Year | Key Parameters | Reference |
|---|---|---|---|
| DA | 2016 | w: 0.9 → 0.4; s, a, c, f, e = 0.1 | [8] |
| RIME | 2023 | NR = 1/√t; E = √(t/T) | [10] |
| DBO | 2023 | $n_1$ = 20%, $n_2$ = 40%, $n_3$ = 30%, $n_4$ = 10% | [9] |
| PO | 2024 | 4 behaviors; uniform random selection | [11] |
| ARO | 2022 | φ(t) = (1−t/T)^(2t/T); k = randi(dim) | [12] |
| INFO | 2022 | 3 elites; $w_1$, $w_2$, $w_3$ ∈ [0, 2] random | [13] |
| GTO | 2021 | p = 0.03; $W_0$ = 0.8, decay = 0.98/iter | [14] |

## REFRENCES

[1] Ahmad, S., Chipperfield, A., & Tokhi, O. (2000). Dynamic modelling and optimal control of a twin rotor MIMO system. In Proceedings of the IEEE National Aerospace and Electronics Conference (NAECON) (pp. 391–398).
[2] Lopez-Martinez, M., Ortega, M. G., Vivas, C., & Rubio, F. R. (2007). Nonlinear $L_2$ control of a laboratory helicopter with variable speed rotors. Automatica, 43(4), 655–661.
[3] Apkarian, H., & Bompart, V. (2007). Non-smooth structured control design with application to PID loop-shaping of a process. International Journal of Robust and Nonlinear Control, 17(14), 1320–1342.
[4] Bryson, A. E., & Ho, Y.-C. (1975). Applied optimal control: Optimization, estimation and control. New York, NY: Taylor & Francis.
[5] Levine, W. (1996). The control handbook. Boca Raton, FL: CRC Press.
[6] Hossain, M. A., Islam, M. S., & Islam, T. (2018). Genetic algorithm based optimal LQR controller for helicopter. International Journal of Advanced Computer Science and Applications, 9(8), 226–232.
[7] Abdel-Raouf, O., Abdel-Baset, M., & El-Henawy, I. (2014). An improved swarm optimization for parameter estimation and longitudinal data analysis of a flexible robot arm. International Journal of Computer Applications, 101(9), 1–6.
[8] Mirjalili, S. (2016). Dragonfly algorithm: A new meta-heuristic optimization technique for solving single-objective, discrete, and multi-objective problems. Neural Computing and Applications, 27(4), 1053–1073.
[9] Xue, J., & Shen, B. (2023). Dung beetle optimizer: A new meta-heuristic algorithm for global optimization. Journal of Supercomputing, 79, 7305–7336.
[10] Su, H., Zhao, D., Heidari, A. A., Liu, L., Zhang, X., Mafarja, M., & Chen, H. (2023). RIME: A physics-based optimization. Neurocomputing, 532, 183–214.
[11] Lian, J., Hui, G., Ma, L., Zhu, T., Wu, X., Heidari, A. A., Chen, Y., & Chen, H. (2024). Parrot optimizer: Algorithm and applications to medical problems. Computers in Biology and Medicine, 172, 108064.
[12] Wang, L., Cao, Q., Zhang, Z., Mirjalili, S., & Zhao, W. (2022). Artificial rabbits optimisation: A new bio-inspired meta-heuristic algorithm for solving engineering optimisation problems. Engineering Applications of Artificial Intelligence, 116, 105082.
[13] Ahmadianfar, I., Heidari, A. A., Noshadian, S., Chen, H., & Gandomi, A. H. (2022). INFO: An efficient optimization algorithm based on weighted mean of vectors. Expert Systems with Applications, 195, 116516.
[14] Abdollahzadeh, B., Gharehchopogh, F. S., & Mirjalili, S. (2021). Gorilla troops optimizer: A new nature-inspired metaheuristic algorithm for global optimization problems. Knowledge-Based Systems, 228, 107535.

[15] Hansen, N., Müller, S. D., & Koumoutsakos, P. (2003). Reducing the time complexity of the derandomized evolution strategy with covariance matrix adaptation (CMA-ES). Evolutionary Computation, 11(1), 1–18.
[16] Cabecinhas, D., Cunha, R., & Silvestre, C. (2015). A globally stabilizing path following controller for rotorcraft with wind disturbance rejection. IEEE Transactions on Control Systems Technology, 23(2), 708–714.
[17] Ahmad, M. A., Raja Ismail, R. M. T., & Ramli, M. S. (2010). Control strategy of Buck converter driven DC motor: A comparative assessment. Australian Journal of Basic and Applied Sciences, 4(10), 5002–5020.
[18] Ziegler, J. G., & Nichols, N. B. (1942). Optimum settings for automatic controllers. Transactions of the ASME, 64, 759–768.